ISSN 0023-1584, Kinetics and Catalysis, 2010, Vol. 51, No. 5, pp. 704–709. © Pleiades Publishing, Ltd., 2010.
Original Russian Text © V.O. Dundich, S.A. Khromova, D.Yu. Ermakov, M.Yu. Lebedev, V.M. Novopashina, V.G. Sister, A.I. Yakimchuk, V.A. Yakovlev, 2010, published in Kinetika i Kataliz, 2010, Vol. 51, No. 5, pp. 728–734.

Nickel Catalysts for the Hydrodeoxygenation of Biodiesel

V. O. Dundich[a], S. A. Khromova[b], D. Yu. Ermakov[b], M. Yu. Lebedev[b], V. M. Novopashina[b], V. G. Sister[c], A. I. Yakimchuk[d], and V. A. Yakovlev[a]

[a] *Novosibirsk State University, Novosibirsk, 630090 Russia*
[b] *Boreskov Institute of Catalysis, Siberian Branch, Russian Academy of Sciences, Novosibirsk, 630090 Russia*
[c] *Moscow State University for Engineering Ecology, Moscow, 107884 Russia*
[d] *Frumkin Institute of Physical Chemistry and Electrochemistry, Russian Academy of Sciences, Moscow, 119991 Russia*
e-mail: dundich@catalysis.ru

Received October 27, 2009

Abstract—A number of nickel and nickel–copper catalysts for the hydrodeoxygenation of fatty acid esters (biodiesel) were studied. The CeO_2 and ZrO_2 oxides and the CeO_2–ZrO_2 binary system were used as supports. The Ni–Cu/CeO_2–ZrO_2 catalyst exhibited the highest activity; it allowed us to quantitatively convert biodiesel into linear alkanes under mild conditions (290–320°C, 1.0 MPa). It was found that the selectivity of the formation of the main product (heptadecane) was 70–80%. The main correlations between the nature of catalysts and their activity under conditions of the target reaction were determined using temperature-programmed reduction, X-ray diffraction analysis, and electron microscopy. It was hypothesized that the high activity of Ni–Cu/CeO_2–ZrO_2 in the test reaction can be explained by the presence of a $Ni_{1-x}Cu_x$ ($x = 0.2$–0.3) solid solution as a constituent of the active component of the catalyst.

DOI: 10.1134/S0023158410050113

INTRODUCTION

Recently, biomass has been considered as an alternative to traditional fossil energy carriers–petroleum, natural gas, and coal [1–3]. Processes for the production of not only various kinds of fuel (fuel biogas and synthesis gas [4, 5], liquid fuels [1, 6], transport fuels [7, 8]) but also valuable chemical products [3–6] have been developed worldwide.

The manufacture of diesel fuel (biodiesel and so-called green diesel) from vegetable oils and animal fats is an intensively developed area of bioenergetics. Biodiesel is a mixture of the methyl esters of fatty acids from the series C_{18}–C_{20}; it is used as an additive (no more than 20%) to improve traditional diesel fuels [9]. Green diesel is a deeper conversion product of the initial fatty acid triglycerides; it is a mixture of alkanes from the series C_{14}–C_{19}, which are characterized by a high cetane number and can be used as improving additives to traditional diesel fuel. The C_{14}–C_{19} alkanes of biological origin can be prepared by both the hydrocracking of fatty acid triglycerides [10] and the hydrodeoxygenation of biodiesel [11].

Traditional desulfurization catalysts—sulfidized Ni–Mo/Al_2O_3 and Co–Mo/Al_2O_3 —have been most frequently used in the above processes [12]. However, because of a low sulfur content of the starting raw material of plant origin, these catalysts are rapidly deactivated as a result of the reduction and subsequent carbonization of an active component [13]. Catalysts based on Pd, Pt, Ru, and Rh noble metals have been used in the hydrocracking and hydrodeoxygenation of esters [14–16]. However, the use of these catalysts in large-scale processes is not promising because they are expensive. Thus, it seems reasonable to develop catalysts free of noble metals for the mild hydrocracking of lipid derivatives of plant origin. As found previously [17], the deoxygenation of aromatic and aliphatic oxygen-containing compounds to corresponding hydrocarbons can be efficiently performed on nickel catalysts.

The aim of this work was to develop and characterize nickel catalysts for the hydrodeoxygenation of fatty acid esters (biodiesel). The ZrO_2 and CeO_2 oxides and the ZrO_2–CeO_2 mixed oxide were chosen as supports for the catalysts. The support was chosen based on the assumption that the ZrO_2 and CeO_2 oxides have active sites with labile oxygen, at which additional activation of oxygen-containing compounds can take place.

EXPERIMENTAL

Nickel-containing catalysts were synthesized by coprecipitation from a mixture of the solutions of nickel, copper, cerium, and zirconium nitrates with a solution of sodium hydroxide followed by granulation and thermal treatment in accordance with a published procedure [18]. A series of samples with various component concentrations was prepared. Table 1 summarizes the texture characteristics of these samples.

The hydrodeoxygenation catalysts were tested in a fixed-bed reactor at 290–400°C and a total pressure of 1.0 MPa. A catalyst portion of 1.5 ml (particle size of

0.2–0.5 mm) was diluted with 0.5 ml of quartz sand with the same particle size and loaded into the reactor. The flow rates of supplied gases (H_2 + Ar) were 10 l/h each. Biodiesel was supplied to the reactor at a rate of 3 ml/h. At the reactor outlet, a portion of products was condensed in a trap thermostated at 50°C. These products were subsequently analyzed on a CHROMOS GC 1000 chromatograph with a Zebron ZB-5 capillary column (stationary phase, 5% phenyl + 95% dimethylpolysiloxane; column length, 30 m; inner diameter, 0.32 mm; phase thickness, 0.25 mm). The on-line analysis of the gas phase (H_2, CO, CO_2, and CH_4) was performed on the same chromatograph with the use of columns packed with Silochrom (column length, 3 m; inner diameter, 2 mm) and thermal conductivity and flame-ionization detectors (TCD and FID, respectively).

The catalysts were studied by temperature-programmed reduction (TPR) in a flow of a gas mixture of H_2 (10%) and Ar (90%) at a flow rate of 40 ml/min. The weight of a catalyst portion was 0.2 g. The samples were placed in a U-shaped quartz reactor and heated in a reductive atmosphere to 700°C at a rate of 5 K/min. The concentration of hydrogen in the mixture at the reactor outlet was measured using a TCD.

X-ray diffraction (XRD) analysis was also used in catalyst characterization. A Siemens D500 diffractometer (Germany) with monochromated CuK_α radiation ($\lambda = 1.5418$ Å) was used at a step of $2\theta = 0.05°$ and an accumulation time of 5 s at each point. A special high-temperature reactor chamber was developed at the Boreskov Institute of Catalysis, Siberian Branch, Russian Academy of Sciences to perform in situ XRD analysis. The rate of heating was 25 K/min; the pressure of hydrogen was 1 atm, and the flow rate of hydrogen (the only gas-phase component) was 600 cm^3/min. At 300°C, we began to measure diffraction patterns over the range of $2\theta = 30°–55°$ and continued the measurement until the pattern became unchanged. Then, the chamber was cooled in a flow of hydrogen, and the measurement was performed once again over the range of $2\theta = 30°–80°$.

The crystal lattice parameters were calculated by the least-squares technique using the Polikristall program. The size of the coherent scattering domain (CSD) was determined from the Selyakov–Scherrer equation [1] based on the integral widths of diffraction lines:

$$D_{hkl} = \frac{\lambda}{\beta\cos\theta}, \quad (1)$$

where λ is the wavelength; D_{hkl} is the effective crystallite size, which depends on the shape of the crystallite and the direction [hkl]; and β is the integral line width.

The samples were studied by high-resolution transmission electron microscopy (TEM) on a JEM-2010 transmission electron microscope (JEOL, Japan) with an accelerating voltage of 200 kV and a resolution of 0.14 nm.

Table 1. Composition and texture characteristics of nickel catalysts for the hydrodeoxygenation of biodiesel

Catalyst	Specific surface area S_{BET}, m^2/g	Elemental composition, %
Ni–Cu/ZrO_2–CeO_2	141	Cu – 10.4, Ni – 30.3, CeO_2 – 17.5, ZrO_2 – 28.0
Ni–Cu/CeO_2	140.6	Cu – 13.6, Ni – 29.9
Ni–Cu/ZrO_2	141.8	Cu – 2.64, Ni – 9.76
Ni/CeO_2	139.9	Ni – 31.6
Ni/ZrO_2	122.4	Ni – 38.8

RESULTS AND DISCUSSION

Study of Biodiesel Hydrodeoxygenation Products

To determine the effect of the nature of the catalyst on its activity in the hydrodeoxygenation of fatty acid methyl esters, we prepared a series of nickel and nickel–copper catalysts supported on Ce and Zr oxides. First, we attempted to optimize the composition of an active component in nickel and nickel–copper catalysts. Previously [18], it was demonstrated that copper considerably affects the activity and selectivity of nickel catalysts for the hydrogenolysis of oxygen-containing organic compounds. It was reasonable to expect a considerable effect of copper on the hydrodeoxygenation of fatty acid esters. In addition, it was necessary to determine how the supports (cerium and zirconium oxides) affected the activity of the catalyst. In general, the series of prepared catalysts consisted of the following samples: Ni/ZrO_2, Ni/CeO_2–ZrO_2, Ni–Cu/CeO_2, Ni–Cu/ZrO_2, Ni–Cu/CeO_2–ZrO_2, and CeO_2–ZrO_2.

Figure 1 shows how the yield of biodiesel hydrodeoxygenation products in the presence of nickel and nickel–copper catalysts depends on reaction temperature. Linear alkanes from the series C_{12}–C_{17}, methane, and H_2O were the main products on all of the catalysts tested. Carbon oxides were not detected among gaseous reaction products, and this is reasonable because CO and CO_2 were reduced to methane under process conditions on nickel catalysts [19].

An analysis of the distribution of liquid hydrodeoxygenation products demonstrated that heptadecane was the main product, which was formed with 70–75% selectivity. Based on the experimental data, we proposed the following reaction scheme for the conversion of fatty acid methyl esters (using methyl oleate as an example):

1. Double bond hydrogenation

$$\underset{\text{methyl oleate (biodiesel)}}{H_3C(CH_2)_7CH{=}CH(CH_2)COOCH_3} \xrightarrow{+H_2} \underset{\text{methyl stearate}}{C_{17}H_{35}COOCH_3}.$$

2. Ester group elimination by C–O bond hydrogenolysis or ester group decarboxylation followed by CO_2 formation

$$C_{16}H_{33}CH_2COOCH_3 \xrightarrow{+H_2} C_{18}H_{38} + 2H_2O + CH_4$$
$$\xrightarrow{+H_2} C_{17}H_{36} + CO_2 + CH_4,$$
$$CO_2 + H_2 \longrightarrow CH_4 + H_2O.$$

3. Hydrocracking of terminal C–C bonds in alkanes

$$C_{17}H_{36} \xrightarrow[-CH_4]{+H_2} C_{16}H_{34} \xrightarrow[-CH_4]{+H_2} C_{15}H_{32} \xrightarrow[-CH_4]{+H_2} \ldots.$$

At temperatures higher than 300°C, the conversion of methyl esters was higher than 90% in all cases.

The yield of methane increased with reaction temperature. However, biodiesel methanization on monometallic nickel catalysts (Ni/ZrO_2 and Ni/CeO_2–ZrO_2) occurred at lower temperatures than on nickel–copper catalysts. Thus, the quantitative formation of methane from biodiesel on nickel catalysts occurred even at 300°C, whereas complete biodiesel methanization on nickel–copper samples was observed only above 410°C. Thus, the introduction of copper into the catalyst makes it possible to perform biodiesel hydrodeoxygenation over a wider range of temperatures. In this case, as found previously [18, 20], copper itself is inactive in the hydrodeoxygenation of oxygen-containing organic compounds.

Thus, to explain the reasons for the catalytic effect of nickel systems in the test reaction, it was necessary to perform additional studies with the use of a number of physicochemical techniques.

Study of Nickel Catalysts for Biodiesel Hydrodeoxygenation

The TPR method allowed us to determine the temperature of the reduction of oxidized catalyst species. Figure 2 shows the TPR curves of the test catalysts and supports. As can be seen, each particular curve exhibits a characteristic temperature region of hydrogen consumption: 150–350 or 300–500°C for the nickel–copper systems or nickel catalysts, respectively. It was

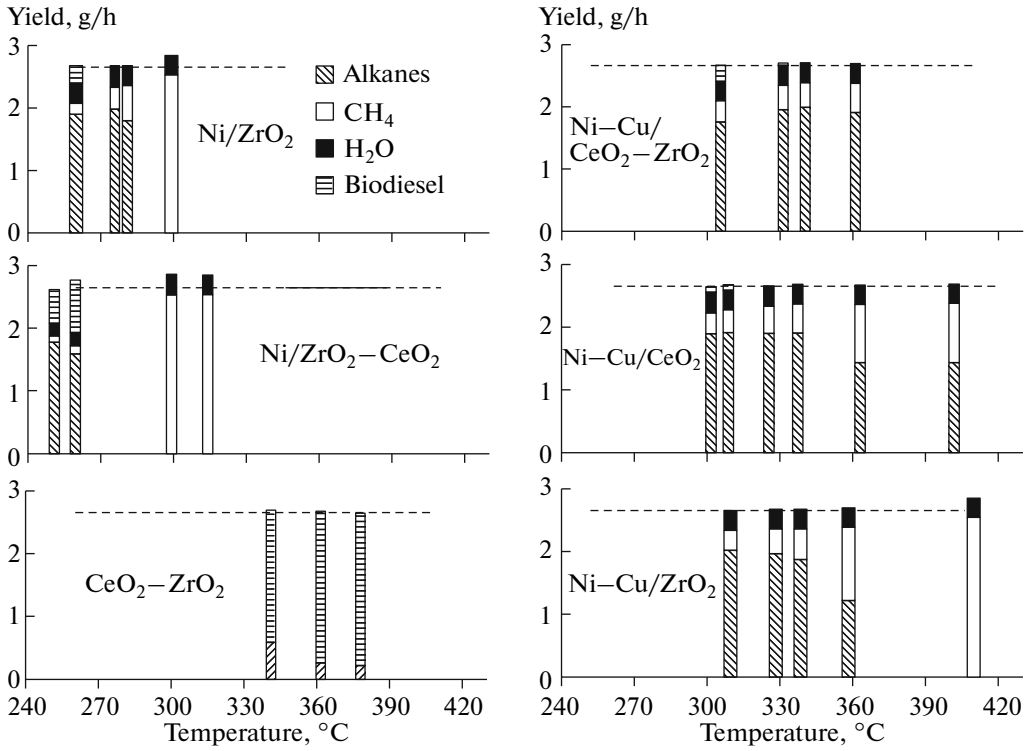

Fig. 1. Yields of the reaction products of biodiesel hydrodeoxygenation on nickel and nickel–copper catalysts at various temperatures and a liquid hourly space velocity (LHSV) of 2 h^{-1}. The horizontal dashed line shows the initial biodiesel consumption of 2.76 g/h.

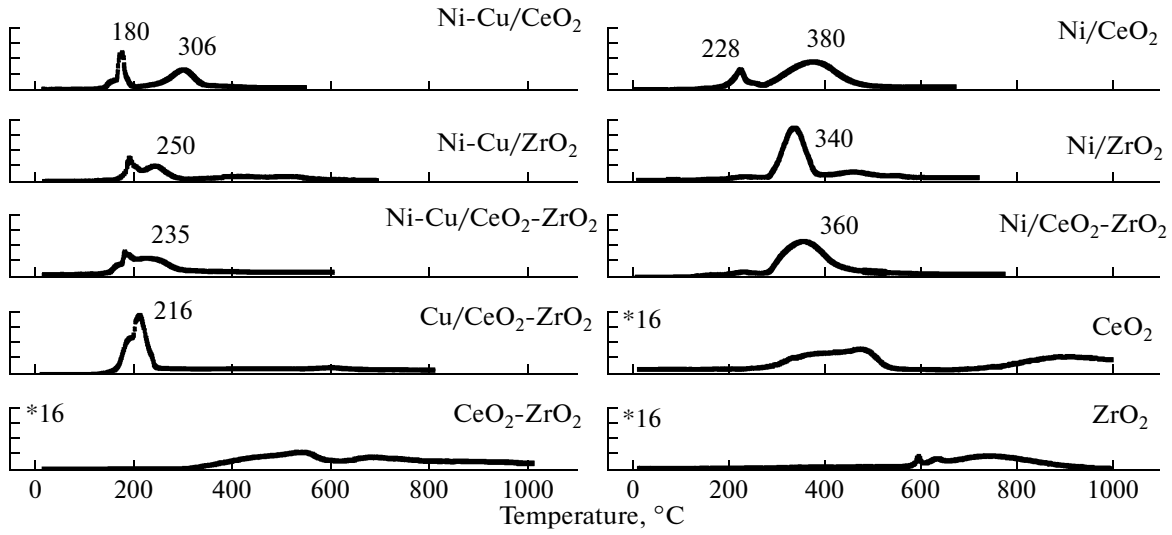

Fig. 2. TPR curves of hydrodeoxygenation catalysts and CeO_2, ZrO_2, and CeO_2–ZrO_2 supports.

hypothesized that the reduction of metal oxides to a metal state occurred in these regions.

For nickel catalysts, an absorption maximum was observed at temperatures from 340 to 380°C depending on the nature of the support. The introduction of copper makes it possible to decrease the reduction temperature of a nickel oxide phase, on the average, by 100°C. Copper oxide, as such, is reduced to a metal state at 180–200°C [16]. Apparently, copper metal activates adsorbed molecular hydrogen, which, in turn, is responsible for the reduction of nickel oxide at lower temperatures.

Supports with no active component (CeO_2–ZrO_2, CeO_2, and ZrO_2) absorb much smaller hydrogen amounts than nickel catalysts. The absorption of hydrogen by cerium oxide and a mixed cerium–zirconium oxide was observed in the temperature range of 300–600°C, which likely corresponds to the partial reduction of surface cerium oxide. The further reduction of ZrO_2 occurred at higher temperatures (600–900°C).

Table 2. Crystal unit cell parameters and particle size (CSD) in unreduced and reduced samples

Catalyst	Initial sample			Reduced sample		
	phase composition	CSD (D), Å	unit cell parameter a, Å	phase composition	CSD (D), Å	unit cell parameter a, Å
$NiCu/CeO_2$	NiO	110		$Ni_{0.8}Cu_{0.2}$	130	3.542(1)
	CuO	300		Cu	350	3.617(2)
	CeO_2		5.417(3)	CeO_2		
$NiCu/ZrO_2$	NiO	40		$Ni_{0.8}Cu_{0.2}$	120	3.544(2)
	$CaCO_3^*$			$CaCO_3$		
	ZrO_2			ZrO_2		
$NiCu/CeO_2$–ZrO_2	NiO	40		$Ni_{0.7}Cu_{0.3}$	100	3.551(4)
	$CaCO_3^*$			$CaCO_3$		
	$Ce_xZr_{1-x}O_2$			$Ce_xZr_{1-x}O_2$		

* 3% $CaCO_3$ was present as an impurity in the precursor of ZrO_2.

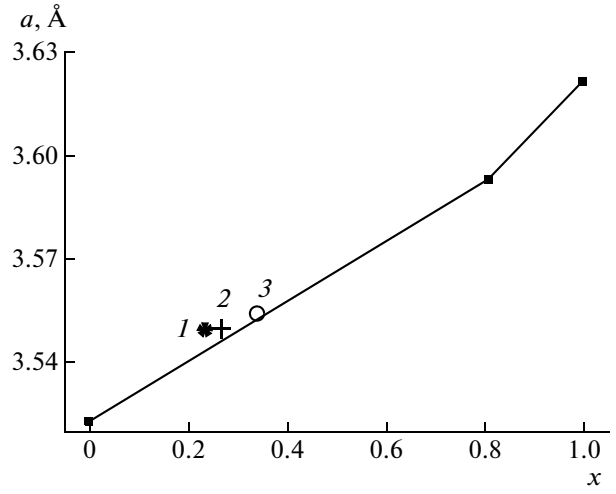

Fig. 3. Unit cell parameter of the $Ni_{1-x}Cu_x$ solid solution as a function of x based on our data and the Powder Diffraction File (Ni, PDF no. 040850; Cu, PDF no. 040836; and $Cu_{0.81}Ni_{0.19}$, PDF no. 471406). Samples: (*1*) reduced Ni–Cu/CeO_2, (*2*) reduced Ni–Cu/ZrO_2, and (*3*) reduced Ni–Cu/CeO_2–ZrO_2.

Because the catalysts underwent a structure and phase rearrangement upon reduction under hydrodeoxygenation conditions (280–380°C; H_2 pressure of 0.25–1.0 MPa), it was important to determine their phase composition under real catalytic reaction conditions. In this connection, we performed a series of experiments, in which the samples were studied in situ by XRD analysis in a flow of hydrogen at 300°C and a pressure of 1.0 atm. From the XRD patterns of the initial Ni–Cu/CeO_2, Ni–Cu/ZrO_2, and Ni–Cu/CeO_2–ZrO_2 samples, it follows that the reflections of CeO_2 and NiO phases were present in these patterns. Upon reduction, the reflections of nickel oxide disappeared and reflections due to a metal phase appeared.

Table 2 summarizes the phase composition, parameters, and average CSD sizes of individual phases in the test catalysts. As a result of reduction, the particle size of an active component increased because of the formation of new nickel and copper metal phases. The average CSD size of metal particles was 100–130 Å.

A $Ni_{1-x}Cu_x$ solid solution was detected in the reduced samples. To determine its composition, we plotted the dependence of x on the unit cell parameter with the use of published data (Fig. 3). Comparing the results obtained, we can conclude that the unit cell parameter a = 3.542(1) Å of the reduced Ni–Cu/CeO_2 sample (sample 1) corresponds to $x = 0.2$ in the formula $Ni_{1-x}Cu_x$. In the reduced Ni–Cu/ZrO_2 sample (sample 2), the unit cell parameter of 3.544(2) Å also corresponds to $x = 0.2$, and a = 3.551(4) Å in Ni–Cu/CeO_2–ZrO_2 (sample 3) corresponds to x = 0.3. In this case, note that the Ni–Cu/CeO_2–ZrO_2 catalyst exhibited the highest activity. It is likely that differences in the composition of $Ni_{1-x}Cu_x$ solid solutions in the test catalysts are responsible for their activity in the hydrodeoxygenation of fatty acid esters.

The results of XRD analysis were supported by data obtained by high-resolution TEM for the reduced Ni–Cu/CeO_2–ZrO_2 sample. The micrographs (Fig. 4) indicate that the active catalyst component had the form of disordered crystallite particles with variable composition of size from 50 to 300 Å. The catalyst surface was almost completely covered with these particles.

A nickel–copper phase with the ratio Ni/Cu = 2.2 : 1 and an interplanar spacing of 2.065 Å, which corresponds to the unit cell parameter a = 3.576 Å, was also detected by electron microscopy. According to XRD data (Table 2), the parameter a of the Ni–Cu phase of the reduced Ni–Cu/CeO_2–ZrO_2 catalyst is 3.551 Å. Thus, the discrepancy between TEM and XRD data is smaller than 0.7%; this demonstrates the reliability of the experimental results.

According to the results of integral energy dispersive X-ray analysis based on a spectrum measured from a large catalyst surface, the atomic concentrations of Ni, Cu, Zr, and Ce on the catalyst surface were 72.3, 22.5, 3.8, and 1.4%, respectively.

Thus, we found that nickel catalysts supported on cerium and zirconium oxides exhibited considerable activity in the hydrodeoxygenation of fatty acid methyl esters (biodiesel). In the test series of catalysts, Ni–Cu/CeO_2–ZrO_2 exhibited the highest activity. It is likely that its high activity can be explained, on the one hand, by the occurrence of a mixed phase of cerium and zirconium oxides and, on the other hand, by the formation of a $Ni_{1-x}Cu_x$ solid solution with x = 0.3 upon reduction.

Using TPR, XRD analysis, and TEM, we found that the introduction of copper into a nickel catalyst facilitated the formation of a $Ni_{1-x}Cu_x$ solid solution with the parameter x = 0.2–0.3. Because of this, the reduction of nickel oxide occurred at temperatures of 280–320°C.

The hydrodeoxygenation of fatty acid esters in the presence of the test catalysts is a key step in the manufacture of second-generation biofuel—green diesel, which is a mixture of C_{14}–C_{18} alkanes; it can be used as an additive to improve the quality of traditional diesel fuel of petroleum origin.

ACKNOWLEDGMENTS

This work was performed within the framework of the Federal Goal-Oriented Program "Research and Development in Priority Areas of the Scientific and Technological Complex of Russia in 2007–2012"

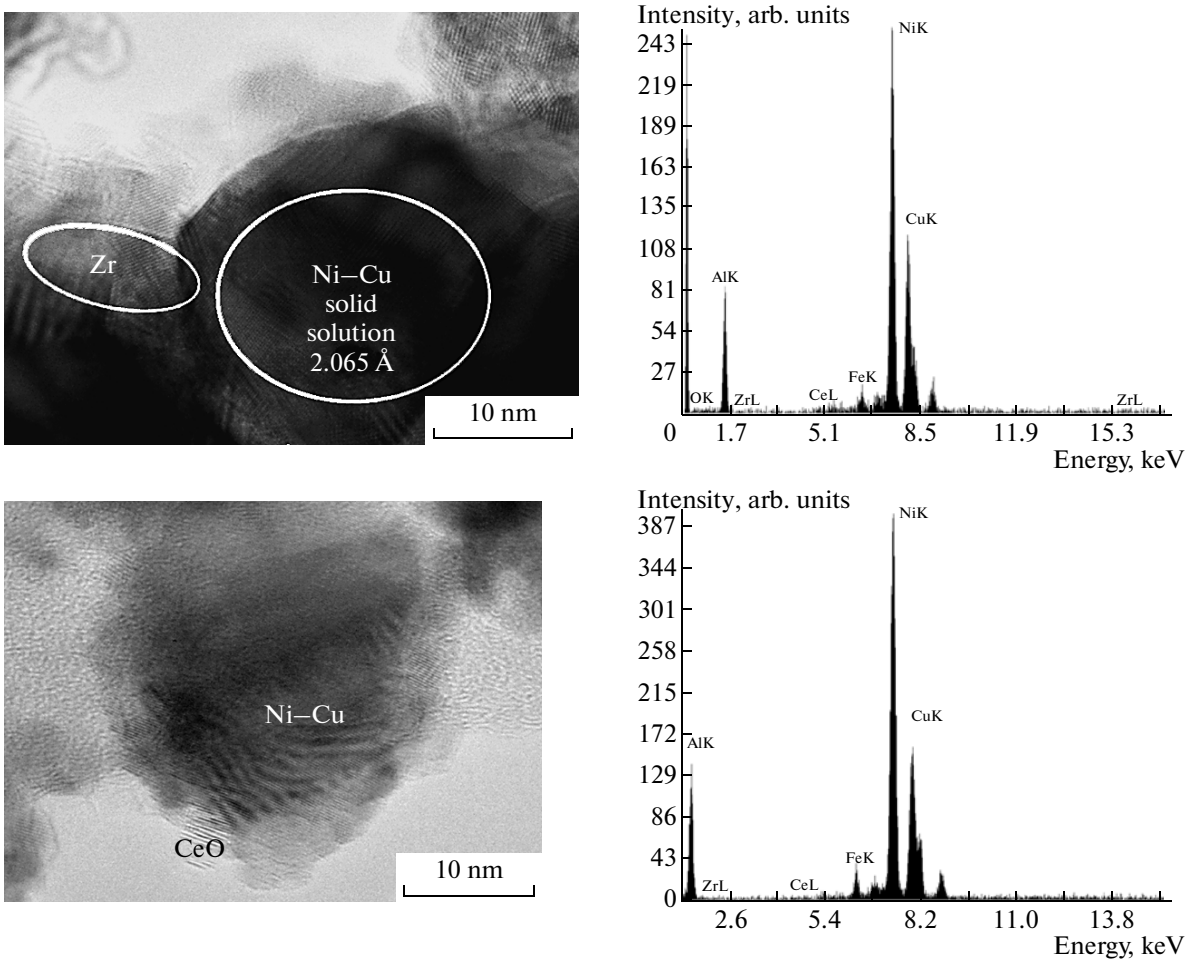

Fig. 4. High-resolution TEM images of a Ni–Cu/CeO_2–ZrO_2 sample (left) as compared with the results of energy dispersive X-ray analysis (EDX) (right).

(state contract no. 02.526.11.6007) and supported by the Federal Goal-Oriented Program "Scientific and Scientific-Pedagogical Cadres of Innovation Russia" for 2009–2013 (state contract no. NK-150P).

REFERENCES

1. Bridgwater, A.V., Meier, D., and Radlein, D., *Org. Geochem.*, *1999*, vol. 30, p. 1479.
2. Sen, Z., *Prog. Energy Combust. Sci.*, 2004, vol. 30, p. 367.
3. Searchinger, T., Heimlich, R., Houghton, R.A., Dong, F., Elobeid, A., Fabiosa, J., Tokgoz, S., Hayes, D., and Yu, T.H., *Science*, 2008, vol. 319, p. 1238.
4. Kirubakaran, V., Sivaramakrishnan, V., Nalini, R., Sekar, T., Premalatha, M., and Subramanian, P., *Renew. Sustain. Energ. Rev.*, 2009, vol. 13, p. 179.
5. Saxena, R.C., Seal, D., Kumar, S., and Goyal, H.B., *Renew. Sustain. Energ. Rev.*, 2008, vol. 12, p. 1909.
6. Elliott, D.C., *Energy Fuels*, 2007, vol. 21, p. 1792.
7. Lee, K.W., Yu, J.X., Mei, J.H., Yan, L., Kim, Y.W., and Chung, K.W., *Ind. Eng. Chem.*, 2007, vol. 13, p. 799.
8. Sharma, Y.C., Singha, B., and Upadhyay, S.N., *Fuel*, 2008, vol. 87, p. 2355.
9. Marchetti, J.M., Miguel, V.U., and Errazu, A.F., *Renew. Sustain. Energ. Rev.*, 2007, vol. 11, p. 1300.
10. Di Serio, M., Tesser, R., Pengmei, L., and Santacesaria, E., *Energy Fuels*, 2008, vol. 22, p. 207.
11. Senol, I., Ryymin, E.-M., Viljava, T.-R., and Krause, A.O.I., *J. Mol. Catal. A: Chem.*, 2007, vol. 268, p. 1.
12. Maher, K.D. and Bressler, D.C., *Bioresour. Technol.*, 2007, vol. 98, p. 2351.
13. Furimsky, E., *Appl. Catal., A*, 2000, vol. 199, p. 147.
14. Senol, O.I., Viljava, T.-R., and Krause, A.O.I., *Appl. Catal., A*, 2007, vol. 326, p. 236.
15. Dundich, V.O. and Yakovlev, V.A., *Khim. Interes. Ust. Razv.*, 2009, vol. 17, p. 527.
16. Kubickova, I., Snare, M., Eranen, K., Maki-Arvela, P., and Murzin, D., *Catal. Today*, 2005, vol. 106, p. 197.
17. Yakovlev, V.A., Khromova, S.A., Sherstyuk, O.V., Dundich, V.O., Ermakov, D.Yu., Novopashina, V.M., Lebedev, M.Yu., Bulavchenko, O., and Parmon, V.N., *Catal. Today*, 2009, vol. 144, p. 362.
18. RF Patent 2335340, 2008.
19. Kuz'min, R.I. and Sevost'yanov, V.P., *Ross. Khim. Zh.*, 2000, vol. 44, p. 77.
20. RF Patent 2 356 629, 2009.